PHYSICAL REVIEW B **74**, 224109 (2006)

Structural, thermodynamic, and transport properties of Laves-phase $ZrMn_2$ from x-ray and neutron diffraction and first principles

M. Rotter,[1,*] A. Grytsiv,[1] Xing-Qiu Chen,[1,2] P. Rogl,[1] R. Podloucky,[1] W. Wolf,[3] V. T. Witusiewicz,[4] A. Saccone,[5] H. Noel,[6] M. Doerr,[7] A. Lindbaum,[8] H. Michor,[8] E. Bauer,[8] S. Heathman,[9] W. Kockelmann,[10] and J. Taylor[10]

[1]*Institut für Physikalische Chemie, Universität Wien, Währingerstrasse 42, A-1090 Wien, Austria*
[2]*School of Material and Metallurgy, Northeastern University, Shenyang, People's Republic of China*
[3]*Materials Design, 44, av. F.-A. Bartholdi, 72000 Le Mans, France*
[4]*ACCESS Materials & Processes, Intzestrasse 5, D-52072 Aachen, Germany*
[5]*Dipartimento di Chimica e Chimica Industriale, Universit'a degli Studi di Genova, via Dodecaneso 31, 16146 Genova, Italy*
[6]*Laboratorie de Chimie du Solide et Inorganique Moléculaire, UMR 6511 CNRS Université de Rennes 1, Avenue du Général Leclerc, F-35042 Rennes, France*
[7]*Institut für Festkörperphysik, Technische Universität Dresden, D-01062 Dresden, Germany*
[8]*Institut für Festkörperphysik, Technische Universität Wien, A-1040 Wien, Austria*
[9]*European Commission, JRC, Institute for Transuranium Elements, Postfach 2340, D-76125 Karlsruhe, Germany*
[10]*Rutherford Appleton Laboratory, ISIS Facility, Chilton, OX11 0Qx, United Kingdom*

(Received 30 May 2006; revised manuscript received 19 September 2006; published 26 December 2006)

Recently, the prediction of structural degeneracy for the ground state of $ZrMn_2$ by *ab initio* methods has stimulated research on this system. We investigated the structural and thermodynamic properties by single crystal and powder x-ray diffraction (at zero and high pressure) as well as by neutron powder diffraction, demonstrating that the C14 Laves phase structure is stable down to a temperature of 4.2 K and up to applied pressure of 56 GPa. The bulk modulus and enthalpy of formation (measured by high-temperature drop calorimetric experiments) of $ZrMn_2$ are found to be 150 GPa and -66.6 kJ (mol of f.u.)$^{-1}$, respectively, in nice agreement with the *ab initio* calculated results. The experimental bulk thermal-expansion data of $ZrMn_2$ resembles that of a typical metal. However, the temperature-dependent electrical resisitivity shows that there is a power law with $n \approx 1.1$ at low temperature quite different from simple metals which originates probably from scattering of the charge carriers on the frustrated Mn moments. The phonons have been investigated in detail by comparing results of *ab initio* calculations with neutron spectra and experimental specific-heat data.

DOI: 10.1103/PhysRevB.74.224109 PACS number(s): 61.50.Lt, 63.20.−e, 71.15.Nc

I. INTRODUCTION

Today, about seventy years after Laves, there exists a fairly good knowledge about the basic structural principles of Laves phases, but many questions still remain. Particularly, theoretical concepts on structure-property relations for optimized alloy design are still not well developed. AMn_2-type Laves phase compounds (A is usually a $3d$ or $4f$ element with a larger atomic radius than Mn) exhibit a large diversity of magnetic ground states. For instance, the antiferromagnetic YMn_2 shows a $3d$ heavy fermion behavior[1] and a spin-liquid-like (or spin-singlet-like) state.[1] The compound $ZrMn_2$ has interesting physical and technological properties (e.g., hydrogen storage materials).[2]

$ZrMn_2$ was investigated by Svechnikov and Petkov[3] in the 1970s; they reported a C14-type structure when quenched from the congruent melting point at 1783 K. Thereafter, numerous experiments[4–10] above 870 K confirmed that $ZrMn_2$ crystallizes in the hexagonal C14 Laves-type structure with lattice constants $a=0.4957-0.5052$, and $c=0.8190-0.8295$ nm. Although many experiments were performed, the key properties at low temperature, such as the lattice structure, remain uninvestigated. Theoretical calculations on the electronic structure of C14 $ZrMn_2$ have already been performed by various techniques. Employing the Korringa-Kohn-Rostoker (KKR) method and involving a local-spin density (LSD) approximation Ishida *et al.*[11] claimed paramagnetism with only Mn at $2a$ sites possibly being ferromagnetic. Asano and Ishida obtained a C14 ferromagnetic state, almost degenerate in energy with its paramagnetic state.[12] More recently, Hong and Fu[13] calculated the hydrogen uptake in $ZrMn_2$ and concluded that the possibility of a magnetic ground state cannot be ruled out.

Up to date, no low-temperature experiments (thermal properties, specific heat, etc.) have been performed. Motivated by the *ab initio* calculations predicting unconventional magnetism and structural degeneracy (prediction of a structural phase transition below room temperature) in this system we present an extensive experimental study of the physical properties of this compound.

II. THEORETICAL INVESTIGATION OF STRUCTURAL PROPERTIES

We investigated $ZrMn_2$ based on density-functional calculations,[14,15] and predicted $ZrMn_2$ to be polymorphic at very low temperatures. Degeneracy of at least three crystal structures (C14, C15, C36) was observed, which are distinguished by different stackings of layers. This degeneracy occurs for the ferromagnetic phases being lowest in energy compared to nonmagnetic or selected antiferromagnetic spin orderings. The gain in magnetization energy due to spontaneous spin polarization is different for all investigated structures but just of the right size to cause the degeneracy. The

C15 structure is stable at zero temperature by a very small energy difference, which disappears when pressure is applied. Including the free energies of lattice vibrations we predict a structural phase transition at 160 K from the C15 to the C14 structure. This is the structure which is found experimentally. The structural degeneracy is not due to any instability: the phonon dispersions for the C14 and C15 structures have no soft modes, the energy of formation indicates strong bonding, and the calculated elastic constants for C15 exclude any weakness due to elastic deformations. Finally, the reliability of our calculations is confirmed by comparison to reliable experimental data also for related compounds, such as $ZrFe_2$ and $ZrCr_2$.

III. HOMOGENEITY REGION AND STRUCTURE OF $ZrMn_2$

A. Experimental details

About ten Zr-Mn alloys containing 60–80 at. % Mn were prepared by arc-melting on a water-cooled copper hearth in Ti-gettered argon from elemental ingots with a minimum purity of 99.9 wt %. Weight losses were attributed to evaporation of the manganese and used to correct the nominal composition of the alloys. The as-cast alloys were sealed in quartz tubes and annealed at 900 °C for 100–150 h before quenching in cold water. Based on x-ray-diffraction profiles of as-cast alloys congruent melting of $ZrMn_2$ was established at 67.9 at. % Mn ($Zr_{0.96}Mn_{2.04}$). This composition was selected for subsequent investigations of physical properties and a specimen with a weight of 20 g was prepared in a high-frequency furnace. Single crystals were mechanically isolated from the crushed as-cast alloy $Zr_{32.1}Mn_{67.9}$. Inspection on an AXS-GADDS texture goniometer assured high crystal quality, unit-cell dimensions, and Laue symmetry of the specimens prior to x-ray intensity data collection on a four-circle Nonius Kappa diffractometer equipped with a charge-coupled device (CCD) area detector employing graphite monochromated Mo$K\alpha$ radiation ($\lambda=0.071\,073$ nm). Orientation matrix and unit-cell parameters for a cubic system were derived using the program DENZO.[16] No absorption corrections were necessary because of the rather regular crystal shape and small dimensions of the investigated specimens. The structure was refined with the aid of the SHELXL-97 program.[17]

X-ray powder-diffraction data from as-cast and annealed alloys were collected employing a Guinier-Huber image plate system with Cu-$K_{\alpha1}$ and Fe-$K_{\alpha1}$ radiation ($8°<2\theta<100°$), and a Siemens D5000 instrument with Cu-$K\alpha_{1,2}$ ($10<2\theta<110°$). Precise lattice parameters were calculated by least-squares fits to the indexed 4θ values employing Ge as internal standard ($a_{Ge}=0.565\,790\,6$ nm). Quantitative Rietveld refinement of the x-ray powder-diffraction data was performed with the FULLPROF program,[18] with the use of its internal tables for scattering lengths and atomic form factors.

Light optical microscopy (LOM) on selected compounds, which were polished and etched by standard methods, scanning electron microscopy and electron microprobe analyses (EMPA) based on energy dispersive x-ray spectroscopy [Si(Li) detector; Mn-K_α and Zr-L_α] were used to examine equilibrium composition on a Cambridge stereoscan equipped with a microprobe Oxford model Si(Li)-Tetralink pentafet. A peak from a cobalt-standard was used by a calibration procedure in order to monitor beam current, gain, and resolution of the spectrometer. Pure elements were used as standards to carry out the deconvolution of overlapping peaks and background subtraction. Finally the x-ray intensities were corrected for ZAF (atomic number, absorption, and fluorescence) effects using the INCA-Energy 300 software package (2002INCA).[19] For quantitative EMPA the samples were analyzed employing an accelerating voltage of 20 kV for a counting time of 60 sec. Overall compositions of the samples after EMPA agree with the nominal values within 1 at. %.

B. Results

The room-temperature x-ray single-crystal study confirmed the hexagonal unit cell [$a=0.502\,93(2)$ nm; $c=0.826\,69(3)$ nm] without any indications of superstructure reflections. The intensity refinement clearly revealed isomorphism of the structure of $ZrMn_2$ with the $MgZn_2$ type (C14 Laves type), see Table I. Although the confidence level of the structure determination is very high ($R_F^2=0.024$), antisite atoms or vacancies at a level of about 5% can neither be determined from the refinement of the occupational numbers nor simply be judged from atom displacement parameters—differences involved concern only $\Delta\rho=0.8$ electrons, too low to be discerned from x-ray intensity data. Anisotropic thermal parameters of all atoms display almost spherical atom shapes indicating a rather uniform bonding scheme. This is in line with interatomic distances, which merely reflect the sum of the atom radii.

EMPA of as-cast alloys revealed the homogeneity limits of the $ZrMn_2$-based phase from 66 to 72 at. % Mn. The manganese content in the alloys annealed at 900 °C varies from 66.2 to 72.7 at. % Mn. Thus the established homogeneity region of the Laves phase in the Zr-Mn system is much smaller than reported before.[20,4] Lattice parameters of the solid solution decrease with manganese content from $a=0.504\,19(4)$ nm and $c=0.828\,73(6)$ nm for $Zr_{33.9}Mn_{66.1}$ to $a=0.498\,75(6)$ nm and $c=0.8195(1)$ for $Zr_{27.3}Mn_{72.7}$. Furthermore, congruent melting of this phase was observed at a slightly off-stoichiometric composition $Zr_{32.1}Mn_{67.9}$, confirming the *ab initio* prediction, which shows that the congruent melting point occurs at 32.8 at. % of Zr.[15].)

IV. STRUCTURE UNDER PRESSURE

A. *Ab initio* prediction of pressure induced phase transition

The crossing of energy-volume curves between C14 FM and C15 FM at about 0.0421 nm^3/f.u., and between C14 FM and C36 FM at 0.043 08 nm^3/f.u. indicates that C14 FM and C36 FM structures are energetically favorable under pressures. The optimized total energy E vs V relation was fitted to a fourth-order polynomial $E(V)$ for a given phase. From this we derived the pressure-volume $\left(P=-\frac{\partial E}{\partial V}\right)$ relation which is used to calculate the pressure-dependent enthalpy of for-

TABLE I. Structure parameters obtained from x-ray single-crystal and neutron powder data and details of the refinement procedure for $Zr_{0.96}Mn_{2.04}$. ($MgZn_2$ type, space group $P6_3/mmc$ No. 194, origin at center). Crystal structure data are standardized using the program Structure Tidy. $^\sharp$ Anisotropic atomic displacement parameters U_{ij} in $[10^2\ \mathrm{nm}^2]$.

Parameter/temperature	298 K	293 K	6 K
Lattice parameters $a;c$ (nm)	0.50293(2); 0.82669(3)	0.502978(4); 0.826630(10)	0.501615(4); 0.825481(10)
Data collection	Nonius Kappa/CCD	TOF diffraction	TOF diffraction
Radiation	Mo$K\alpha$	Neutron	Neutron
Reflections measured [total]	$257 \geqslant 4\sigma(F_\alpha)$ of 280 [4100]		
Θ range	$2 \leqslant 2\Theta \leqslant 70$; 180 sec/frame, 144 frames		
Number of variables	11		
$R_{Int}=\Sigma\lvert I_{oB}-I_{cB}\rvert/\Sigma\lvert I_{oB}\rvert$	0.068	0.061	0.044
$R_F^2=\Sigma\lvert F_0^2-F_c^2\rvert/\Sigma\lvert F_0^2\rvert=$	0.024	0.074	0.059
Crystal size	$90\times84\times112\ \mu m^3$		
$R_{wP}=[\Sigma w_i\lvert y_{oi}-y_{ci}\rvert^2/\Sigma w_i\lvert y_{oi}\rvert^2]^{1/2}$		0.038	0.039
Mosaicity; abs. coeff. $[\mathrm{mm}^{-1}]$	<0.45; $\mu=18.80\ \mathrm{mm}^{-1}$		
Extinction (Zachariasen)	0.041(5)		
Goodness of Fit	GOF=1.144	GOF=8.897	GOF=6.399
Atom positions			
Mn1 in $2a$ (0,0,0), occ.	1.00(1) Mn		
U_{eq} (U_{iso}) 10^2 (nm^3)	$U_{eq}^\sharp=0.0063(2)^a$	$U_{eq}^\sharp=0.0066$	$U_{eq}^\sharp=0.0036$
Mn2 in $6h$ $(x,2x,1/4)$, occ.	$x=0.17013(5)$; 1.00(1)Mn	$x=0.16971(1)$	$x=0.16992(2)$
U_{eq} (U_{iso}) 10^2 (nm^3)	$U_{eq}^\sharp=0.0061(2)^b$	$U_{eq}^\sharp=0.0066$	$U_{eq}^\sharp=0.0036$
Zr in $4f$ $(1/3,2/3,z)$, occ.	$z=0.56340(5)$; 1.00(2) Zr	$z=0.56282(6)$	$z=0.56287(6)$
U_{eq} (U_{iso}) 10^2 (nm^3)	$U_{eq}^\sharp=0.0064(2)^c$	$U_{eq}^\sharp=0.0066$	$U_{eq}^\sharp=0.0036$
Residual density; max; min in ($\mathrm{electrons/nm}^3$)$\times1000$	1.51; −1.19		
Interatomic distances (nm)			
Mn1			
−6 Mn	0.25432		
−6 Zr	0.29506		
Mn2			
−2 Mn2	0.24624		
−2 Mn1	0.25432		
−2 Mn2	0.25669		
−6 Zr	0.29503		
Zr			
−6 Mn2	0.29503		
−3 Mn1	0.29506		
−3 Mn2	0.29553		
−1 Zr	0.30871		
−3 Zr	0.30871		

[a] Mn1 ($2a$): $U_{11}=U_{22}=0.0065(2)$; $U_{33}=0.0059(3)$; $U_{13}=U_{23}=0$; $U_{12}=U_{11}$.

[b] Mn2 ($6h$): $U_{11}=0.0063(2)$; $U_{22}=0.0063(2)$; $U_{33}=0.0058(2)$; $U_{13}=U_{23}=0$; $U_{12}=U_{22}$.

[c] Zr ($4f$): $U_{11}=U_{22}=0.0065(2)$; $U_{33}=0.0063(2)$; $U_{13}=U_{23}=0$; $U_{12}=U_{11}$.

mation, $H(P)=E(P)+PV-E_{coh}^{\mathrm{Zr}}-2E_{coh}^{\mathrm{Mn}}$. The pressure-volume equation of states and the enthalpy-pressure relation are shown in Fig. 1. At zero temperature a pressure-reduced phase transformation from C15 FM to C14 FM at 5.9 GPa is predicted.

B. Experiment

High pressure x-ray-diffraction (HPXRD) experiments at ambient temperature were performed at the beamline ID 30 of the European Synchrotron Radiation Facility (ESRF), Grenoble, France. For this purpose a fine powder of $ZrMn_2$

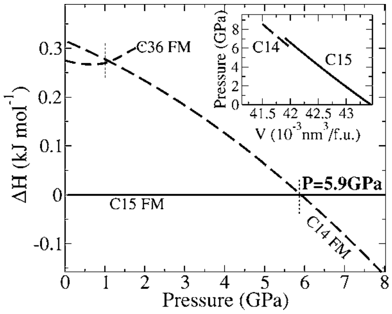

FIG. 1. Calculated enthalpy differences (relative to C15 FM) and equations of state (inset) for $ZrMn_2$ in C14, C15, and C36 FM crystal structures as a function of pressure. Lattice dynamical effects (zero-point and thermal motion of atoms) are not included in these calculations. The enthalpy differences are referenced to the C15 FM structure: $\Delta H = H(P) - H_{C15FM}(P)$.

was loaded in a diamond-anvil cell (DAC), together with a pressure transmitting medium (PTM) and a small ruby crystal for pressure determination (via the ruby fluorescence method). As a PTM silicone oil and N2 were used. The former is easier to handle for experiments at lower pressures, whereas the latter yields better hydrostatic conditions at higher pressures. The x-ray-diffraction patterns at different pressures were then obtained by diffraction of a monochromatic x-ray beam (wavelength 0.020 215 nm) on the sample contained in the DAC, using a two-dimensional (2D) CCD-based detector for capturing the diffraction images. The diffraction rings were then integrated using the FIT2D program,[22] which produced the 1D diffraction patterns used for data analysis.

C. Results

No structural transition was observed up to 56 GPa, the highest pressure which could be reached. The compressibility curve (see Fig. 2) shows a normal behavior with a bulk modulus $B_0 \approx 150$ GPa and $B_0' \approx 4$. These values for the equation of state (EOS) were obtained by fitting the EOS formula of Murnaghan[21] to the experimental data. The experimental value for B_0 is smaller by 30 GPa compared with the *ab initio* calculated result of 180 GPa,[15] due to the fact that *ab initio* calculation underestimates the equilibrium volume by 4% thus resulting in a larger predicted bulk modulus.

The c/a ratio remains unchanged by the application of pressure. Figure 2 shows only the pressure range up to 37 GPa. The data points at higher pressures up to 56 GPa were performed using silicone oil as a PTM, which is strongly nonhydrostatic at such high pressures, and therefore cannot be used for a reliable compressibility curve. However, also the points between 37 and 56 GPa do not indicate any instability of the crystal structure, except a strong broadening of the x-ray lines.

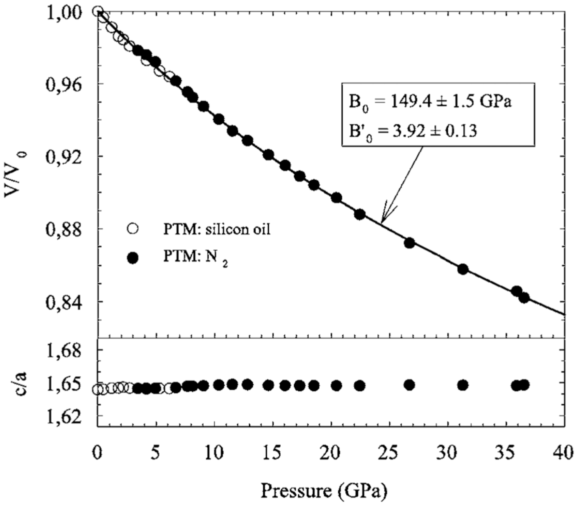

FIG. 2. Relative volume and c/a ratio of the C14 structure of $ZrMn_2$ as a function of pressure up to about 40 GPa. The line shows the result of fitting the Murnaghan EOS formula (Ref. 21) to the experimental data.

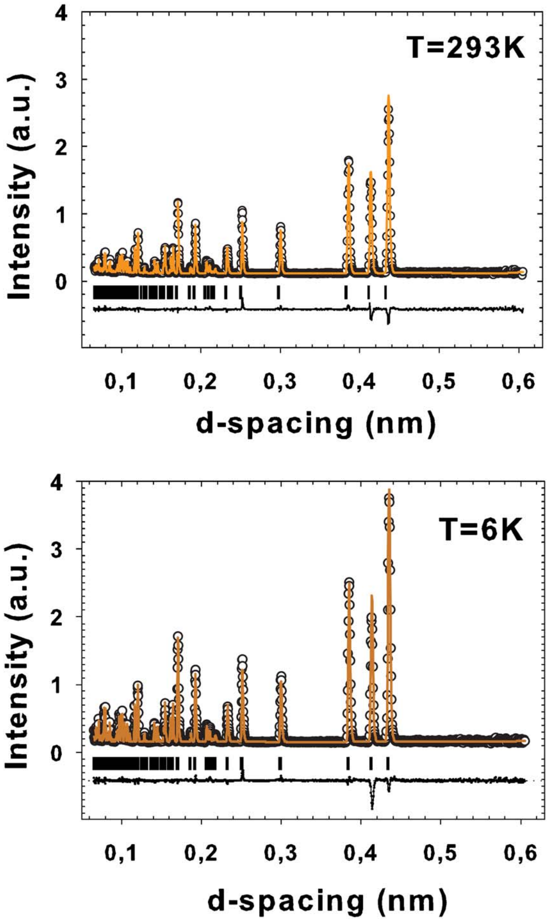

FIG. 3. (Color online) Neutron time-of-flight diffraction pattern of $ZrMn_2$ at T=293 K (top) and 6 K (bottom). The lines indicate a fit from the Rietveld analysis.

V. NEUTRON DIFFRACTION

We collected neutron powder-diffraction data on $ZrMn_2$ on the time-of-flight diffractometer ROTAX at the pulsed neutron spallation source ISIS at the Rutherford Appleton Laboratory, UK. Long runs were carried out at 6 and 293 K

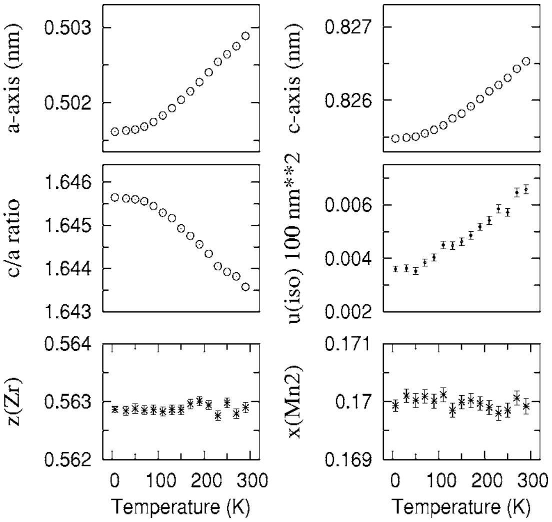

FIG. 4. Temperature dependence of refined structure parameters from neutron powder diffraction: lattice parameters (a,c), ratio (c/a), overall atom displacement parameter (U_{iso}) of Zr and Mn, atomic position parameters z(Zr) and x(Mn2) (compare Table I).

(see Fig. 3), plus short runs at 20-K steps between 6 and 300 K in order to follow the thermal expansion. The data have been fitted according to the Rietveld method using the GSAS program package.[23]

The diffraction patterns do not indicate a structural transition between 6 and 300 K. Figure 4 shows the temperature dependence of the hexagonal lattice parameters a and c as well as the c/a ratio. Between 6 and 290 K the lattice expands in a ($\delta a/a=2.5\times10^{-3}$) and in c ($\delta c/c=1.26\times10^{-3}$), corresponding to a volume change of $\delta V/V=6.26\times10^{-3}$. The volume expansion of the unit cell is displayed in Fig. 5.

The atomic position parameters of Zr and Mn show no dependence on temperature within experimental error (Fig. 4) whereas the overall atom displacement increases with temperature as expected. A weak additional impurity Bragg peak at a d spacing of 0.69 nm is present in the 293 K as well as in the 6-K data. There are no indications of extra magnetic peaks or additional magnetic scattering on top on nuclear Bragg peaks at high d spacings within the experimental error.

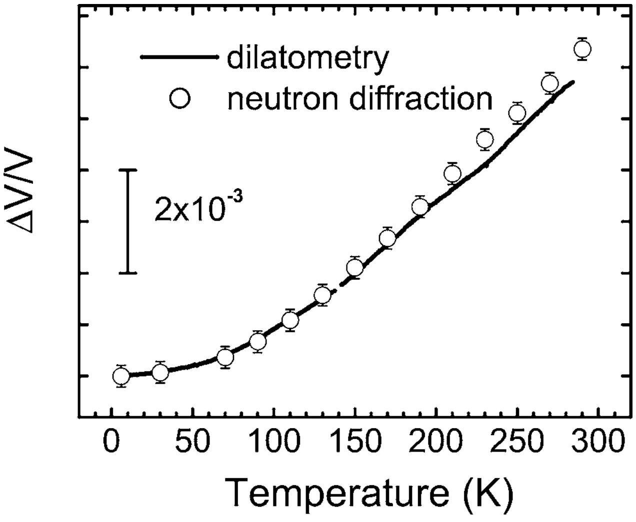

FIG. 5. Volume expansion of $ZrMn_2$ as determined from a dilatometer measurement on a polycrystalline sample (line) in comparison with the volume expansion determined by neutron diffraction (symbols).

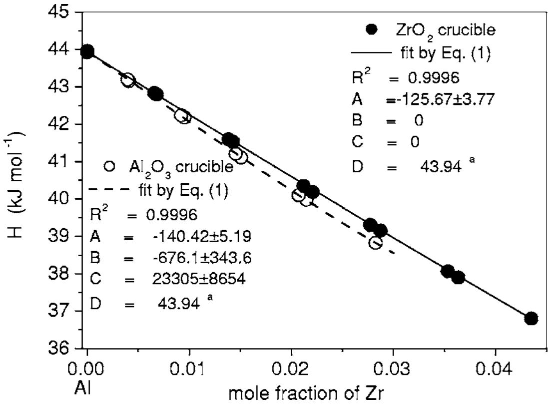

FIG. 6. Measured integral enthalpy of formation of liquid dilute binary Al-Zr alloys due to dropping of solid Al and Zr at 298 K into liquid Al at 1409±5 K. "a" in the figure refers to Ref. 25.

VI. THERMAL EXPANSION

The thermal expansion has been measured using a capacitance miniature dilatometer[24] on a bar-shaped polycrystalline sample with a sample length of 1.39 mm. The force onto the sample was minimized using a very thin spring of only 0.02 mm thickness. For the run shown by the line in Fig. 5 the error bars are about the thickness of the line.

The thermal expansion of $ZrMn_2$ (shown in Fig. 5) resembles that of a typical metal and does not indicate any phase transition in the temperature range between 4 and 300 K. The magnitude of the expansion is only slightly smaller than expected from the temperature dependence of the lattice constants (shown by the symbols in Fig. 5) indicating that in the polycrystalline sample there exists some preferred orientation of the grains (c axis preferred along the measurement direction).

VII. CALORIMETRIC EXPERIMENT

A. Experiment

The heat of dissolution of $Zr_{0.96}Mn_{2.04}$ as well as of pure Zr was measured using an isoperibolic calorimeter by dropping the solid samples at room temperature (i.e., 298 K) into liquid aluminum at a temperature of 1409±5 K. The measurement procedures and the method of evaluation of the integral enthalpy of formation of liquid dilute alloys referred to standard temperature (298.15 K) were described in our previous paper.[35] The value for the enthalpy change upon heating of pure aluminum from room temperature to 1409±5 K ($\Delta H^{1409}_{298,Al}$) was adopted from the Scientific Group Thermodata Europe (SGTE) data for pure elements.[25] Note that this value is required for determination of a calibration factor (heat equivalent) of the calorimeter used.

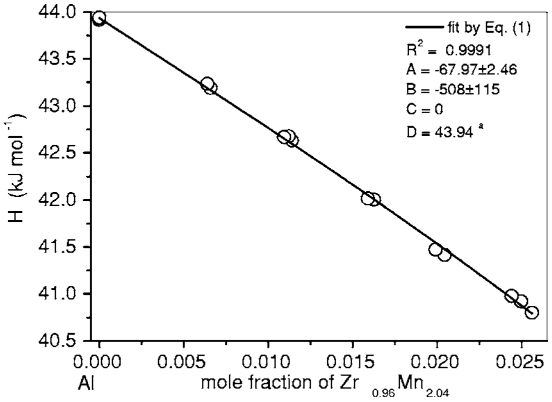

FIG. 7. Integral enthalpy of formation of liquid dilute ternary alloys due to dropping of solid Al and $Zr_{0.96}Mn_{2.04}$ at 298 K into liquid Al at 1409±5 K: points are experimental data; lines result from fitting by Eq. (1).

B. Results and discussion

The calorimetric results concerning the enthalpy of formation of liquid dilute binary Al-Zr alloys and dilute ternary Al-Mn-Zr referred to 298.15 K are shown in Figs. 6 and 7.

Dropping samples of pure Zr (see Fig. 6) and $Zr_{0.96}Mn_{2.04}$ (see Fig. 7) into liquid Al leads to exothermic reactions. The obtained integral values could be fitted properly using the following thermodynamic adapted power series:

$$\Delta H = x(1-x)(A + Bx + Cx^2) + (1-x)D, \qquad (1)$$

where $A-C$ are fitting parameters and D corresponds to $\Delta H^{1409}_{298,\mathrm{Al}}$ according to Ref. 25. The coefficient A denotes the enthalpy of dissolution of the substance i at infinite dilution ($\Delta_{diss}\bar{H}^0_i$). The parameters A of Eq. (1) as determined by least-squares analysis are given in Table II.

1. Enthalpy of dissolution of Zr in liquid Al at different temperatures

The results obtained in the present work for the enthalpy of dissolutions of Zr can be compared with the literature data from various authors measured at various temperatures.

For this purpose, the enthalpy changes upon heating of Zr using the database of Ref. 25 were subtracted from the appropriate parameters A (see Table II) to refer them to equal reference state and the obtained results are plotted as a function of temperature in Fig. 8.

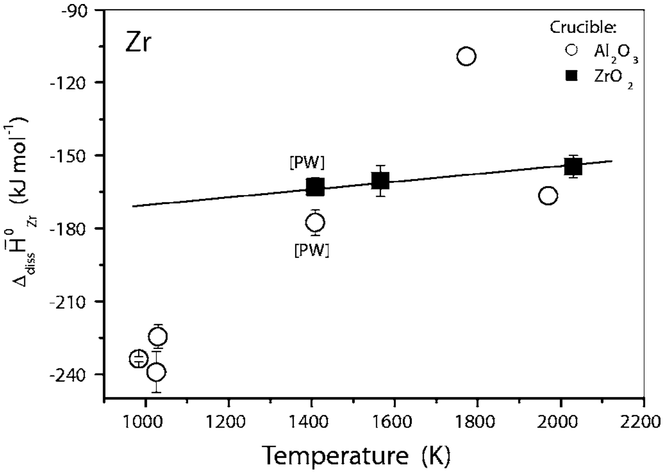

FIG. 8. Comparison of the enthalpy of dissolution of Zr in pure Al measured in the present work [PW] with literature data (Refs. 26–34). Lines result from fitting by Eqs. (2) and (3). Data points refer to liquid Al and solid Zr, respectively.

Several papers deal with the dissolution of Zr (Refs. 26–32 and 34) in liquid aluminum by calorimetry. The data of Batalin *et al.*[32] obtained at 1773 K differ strongly from values of Refs. 30 and 31 and lead to an enormous temperature dependence of the dissolution enthalpy of the elements. Therefore values of Ref. 32 were not taken into consideration. The data obtained for dissolution of Zr using alumina crucibles are more negative than values measured in zirconia crucibles, probably due to a reaction between the Zr sample and the alumina crucible.

For this reason the data obtained in alumina crucibles were not taken into consideration. The remaining data were fitted vs temperature in the given temperature range as

$$\Delta\bar{H}^0_{\mathrm{Zr}} = -181.5 + 0.0133T. \qquad (2)$$

2. Enthalpy of formation

The enthalpy of formation of $ZrMn_{2.04}$ at 298 K was evaluated using the values of parameters from Table II as

TABLE II. Values of fitting parameter A of Eq. (1) (A is equal to partial enthalpy of dissolution in pure Al at infinite dilution, $\Delta_{diss}\bar{H}^0_i$).

Sample	A or $\Delta H^0_{diss,i}$ (kJ mol^{-1})	Error A (2σ) (kJ mol^{-1})	Reference
Al	43.94		25
Mn	−6.84	0.08	35
Zr	−140.42	5.19	Al_2O_3 crucible, present work
Zr	−125.67	3.77	ZrO_2 crucible, present work
$Zr_{0.96}Mn_{2.04}$	−67.97	2.46	present work

$$\Delta_{298}H^0 = \sum_i n_i \Delta_{diss}\bar{H}_i^0 - \Delta_{diss}\bar{H}_{COMP}^0, \tag{3}$$

where $\Delta_{diss}\bar{H}_i^0$ denotes the first partial enthalpy of dissolution in Al of 1 mole of pure substance. n_i is the number of moles of a substance in an intermetallic compound and $\Delta_{diss}\bar{H}_{COMP}^0$ is the first molar enthalpy of dissolution of the intermetallic compound in aluminum. The standard error (2σ) of the enthalpy of formation of the intermetallics was evaluated as

$$2\sigma = \sqrt{\sum_i (n_i E_i)^2 + E_{COMP}^2}, \tag{4}$$

where E_i and E_{COMP} denote the 2σ error for the $\Delta_{diss}\bar{H}_i^0$ and $\Delta_{diss}\bar{H}_{COMP}^0$, respectively. The results of the evaluation is summarized in Table III. The obtained experimental value is in good agreement with the *ab initio* calculated value of -60.9 kJ/mol (Ref. 15).

VIII. TRANSPORT PROPERTIES

The temperature-dependent electrical resistivity $\rho(T)$ of polycrystlline samples is displayed in Fig. 9. $ZrMn_2$ behaves metallic in the temperature range studied. $\rho(T)$ smoothly varies from roughly 195 $\mu\Omega$ cm at room temperature to 44 $\mu\Omega$ cm at 4.2 K. Although $\rho(T)$ of $ZrMn_2$ resembles features of simple metals, the standard Bloch Grüneisen law cannot satisfactorily be applied to describe $\rho(T)$ in the whole temperature range. Particularly the low-temperature range ($T < 10$ K) deviates significantly from simple metals, and within a first approximation there is a power law according to $\rho = \rho_0 + AT^n$ with $n \approx 1.1$ (compare inset, Fig. 9). Normally, simple metals behave at low temperatures like T^5. The observed exponent $n \approx 1.1$ originates probably from scattering of the charge carriers on the frustrated Mn moments.

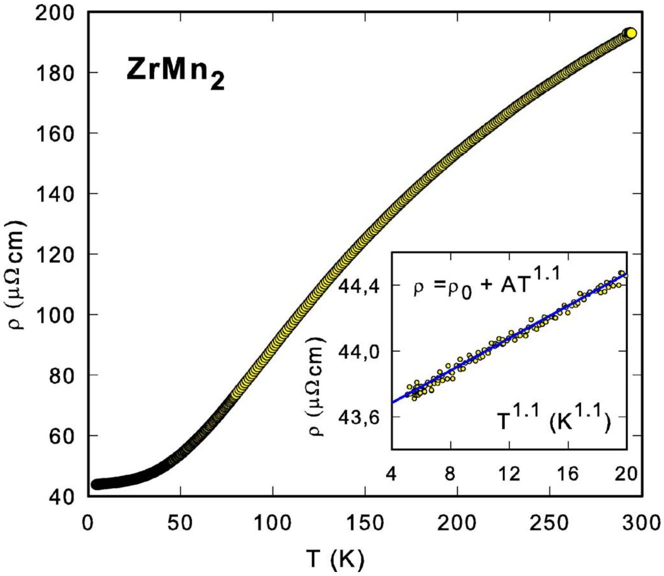

FIG. 9. (Color online) Temperature dependence of the electrical resisitivity of $ZrMn_2$.The inset shows the low-temperature resistivity of $ZrMn_2$ plotted as ρ vs $T^{1.1}$.

IX. HEAT CAPACITY

Specific-heat measurements were carried out on samples of about 1 g in the temperature range 10–170 K employing a quasiadiabatic step heating technique. The temperature-dependent specific heat $C_p(T)$ of a $ZrMn_2$ polycrystal is shown in Fig. 10 as $C_p(T)/T$ vs T. In the temperature interval from about 10 K up to 20 K, $ZrMn_2$ exhibits a regime where the specific heat $C(T)$ behaves like that of a normal metal with $C(T) \sim \gamma T + \beta T^3 + \delta T^5$ revealing a rather large Sommerfeld coefficient $\gamma \simeq 50(5)$ mJ/mol K^2. All three coefficients are of course modified by the magnetic low-temperature contributions, in particular $\beta = 3.5 \times 10^{-5}$ J/mol K^4 and $\delta = 1.25 \times 10^{-7}$ J/mol K^6, and thus not suited for an analysis in terms of the Debye model.

TABLE III. Enthalpy of formation of the intermetallic compounds referred to 298.15 K. Note: The enthalpy of formation is calculated for one formula unit given in the first column.

Compound	$\Delta_{298}H^0$ (kJ mol^{-1})	Error ($\pm 2\sigma$) (kJ mol^{-1})	Reference
$TiMn_2$	-86.76	6.79	35
$Zr_{0.96}Mn_{2.04}$	-66.63	4.44	expt. present work
$ZrMn_2$	-60.9		calc. (Ref. 15)

From the *ab initio* calculated phonon DOS,[36] the phonon heat capacity C_v can be derived from the equation

$$C_v(T) = k_B \int_0^\infty d\omega g(\omega) \left(\frac{\hbar\omega}{k_B T}\right)^2 \frac{\exp(\hbar\omega/k_B T)}{[\exp(\hbar\omega/k_B T) - 1]}, \tag{5}$$

where $g(\omega)$ represents the phonon density of states (DOS) as a function of frequecy ω. The result of this calculation is shown in comparison with the experimental data in Fig. 10. The C14 FM *ab initio* result agrees better with the experimental data.

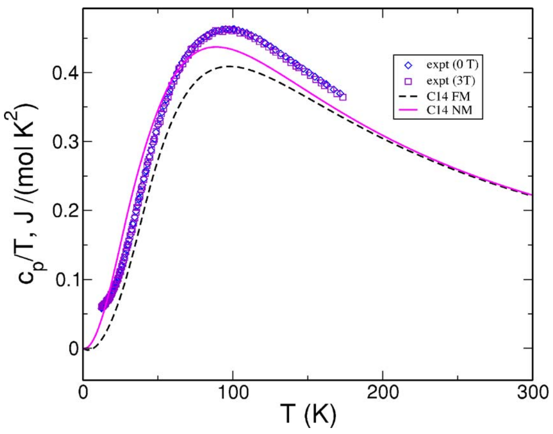

FIG. 10. (Color online) Experimental specific heat of $ZrMn_2$ (data points) in comparison with the calculated phonon contribution for the nonmagnetic and ferromagnetic C14 type of structure (lines).

X. NEUTRON SPECTROSCOPY

Inelastic neutron scattering on powder was used to determine the phonon density of states (PDOS) for $ZrMn_2$ as a function of temperature in order to investigate the possibility of a transition in the lattice dynamics of the system that may be associated with a change in lattice structure. The spectrometer MARI (at the ISIS spallation source, Rutherford Appleton Laboratory) was used as it provides continuous coverage of Q space. A powder sample was mounted in an annular geometry inside a closed-cycle refrigerator. An incident energy of 75 meV was used for this investigation. In order to identify any changes in the lattice dynamics we measured spectra at five temperatures from 15 to 250 K. From the measured double differential scattering cross section $\partial\sigma/\partial\Omega\partial E'$ the scattering function $S(Q,E')$ was calculated according to

$$\frac{\partial\sigma}{\partial\Omega\partial E'} = \frac{k}{k'} S(Q,E'). \tag{6}$$

In this equation k denotes the wave vector of the incoming neutron and k' (E') the wave vector (energy) of the scattered neutron. The data obtained in this way are shown in Fig. 11 and can be compared to the results of the *ab initio* calculated phonon density of states.

The phonon dispersions and phonon densities of states for the C14 structure were derived by making use of the direct method[15,37] based on supercells with periodic boundary conditions. This approach relies on accurately calculated forces but is independent of the actual *ab initio* method. The forces are computed for independent displacements required by the symmetry of the unit cell. Displacement amplitudes of 0.003 nm were chosen. For the calculation of the force constants for the C14 structure the corresponding supercells contain 36 and 24 atoms, and a $3\times3\times3$ $\vec{k}$-point grid was applied. Phonon calculations were done for nonmagnetic as well as ferromagnetic cases.

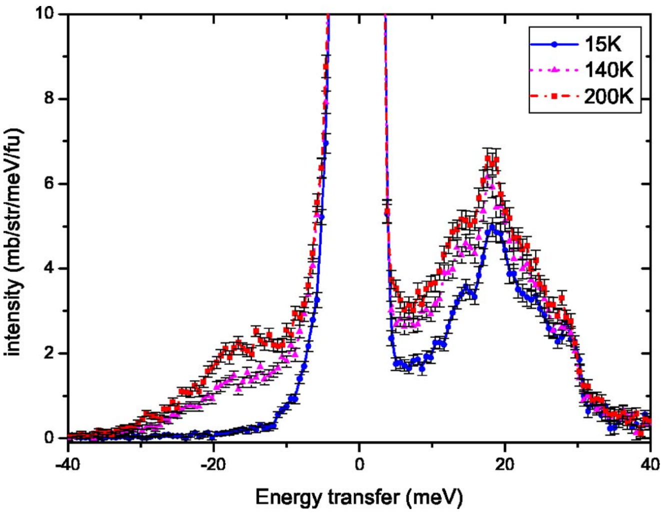

FIG. 11. (Color online) Normalized and background-corrected inelastic neutron-scattering spectra of $ZrMn_2$ taken at MARI with an incident energy of 70 meV at different temperatures. The data shown correspond to the scattering function $S(Q,E)$ and have been averaged over Q from measurements in the Q range of 3.4–107 nm.

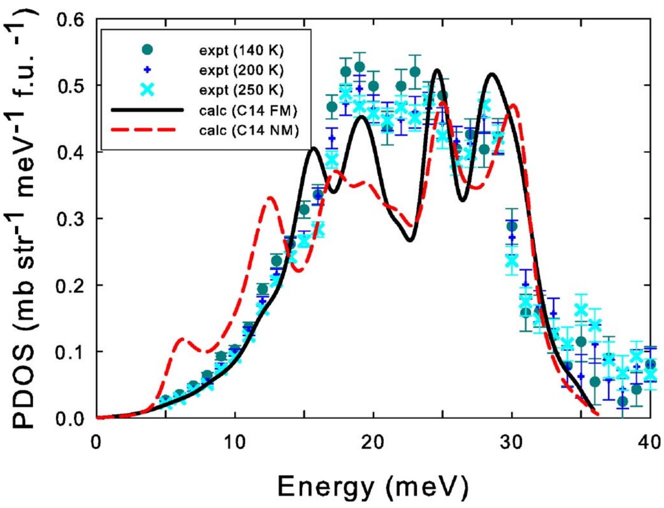

FIG. 12. (Color online) Phonon density of states as calculated from the time-of-flight neutron spectra (MARI, ISIS, UK) in comparison with results of *ab initio* models.

In $ZrMn_2$ the coherent and incoherent neutron cross sections are of comparable magnitude. In the following analysis of the spectra we will assume that the powder average of the polycrystalline cross section gives similar scattering to the incoherent phonon spectrum.

In order to directly compare the calculated phonon density of states with the experimental data, for the calculated PDOS the unit [1/(THz f.u.)] must be converted into mb/(meV steradian f.u.) by

$$\mathrm{PDOS}_{c,\mathrm{ZrMn}_2} = \frac{1}{24\pi}\left(\frac{2\times \mathrm{PDOS}_{\mathrm{Mn}}\times\sigma_{\mathrm{Mn}}}{M_{\mathrm{Mn}}} + \frac{\mathrm{PDOS}_{\mathrm{Zr}}\times\sigma_{\mathrm{Zr}}}{M_{\mathrm{Zr}}}\right), \tag{7}$$

where $\mathrm{PDOS}_{c,\mathrm{ZrMn}_2}$ is the converted total phonon density of states in the unit of mb/(meV steradian f.u.), $\mathrm{PDOS}_{\mathrm{Mn}}$ and $\mathrm{PDOS}_{\mathrm{Zr}}$ are the calculated phonon density of states of Mn and Zr in unit of 1/(THz atom), respectively. σ_{Mn} and σ_{Zr} are the total bound scattering cross sections (σ_{Mn}=2.15 b =2150 mb and σ_{Zr}=6.46 b=6460 mb). M_{Mn} and M_{Zr} correspond to the atomic weight of 54.93 and 91.422 for Mn and Zr, respectively. The resulting PDOS was convoluted with the experimental resolution, a Gaussian with a full width at half maximum of 0.6 meV. In Fig. 12 the calculated PDOS is shown by curves for C14 nonmagnetic (NM) as well as ferromagnetic (FM) $ZrMn_2$.

One may derive the neutron cross section weighted phonon density of states from the measured scattering function $S(Q,E')$ according to

$$\mathrm{PDOS}_{e,\mathrm{ZrMn}_2} = \frac{S(Q,E')\hbar\omega}{Q^2[n(x)+1]} \times \frac{m_n}{\hbar^2}, \tag{8}$$

where $n(x)$ denotes the temperature factor and $x=\frac{\hbar\omega}{k_B T}$ (k_B is Boltzmann constant), the unit of nuclear mass m_n is the constant of $1.660\,56\times10^{-27}$ kg, and $\hbar$ is Planck's constant of

6.5822×10^{-16} eV s$=1.054\,59 \times 10^{-34}$ J s. In Eq. (8) the Debye-Waller factor has been neglected. The symbols in Fig. 12 show the PDOS as determined from the neutron spectra for three different temperatures. This experimental PDOS shows little variation as a function of temperature as expected due to the correction for the Bose factor n.

There are two anomalous features in the PDOS for $ZrMn_2$. (i) The modes at 23 meV and higher energies are predicted to be at higher energies from the *ab initio* model, both from the FM and for the NM calculation. (ii) From the NM calculation two features below 15 meV are predicted, which are not seen in the experiment. The FM calculation does not show such pronounced features and agrees better with the experimental data.

XI. SUMMARY AND OUTLOOK

Magnetic and structural polymorphism is predicted by *ab initio* calculations for the Laves phase compound $ZrMn_2$. The C14, C15, and C36 structures should have very similar enthalpies of formation. A phase transition from the C14 to the C15 structure is predicted at 160 K. Therefore structural properties have been determined by single-crystal and powder x-ray diffraction as well as neutron powder diffraction indicating that the C14 crystal structure is stable down to a temperature of 4.2 K and up to an applied pressure of 56 GPa. No evidence for the magnetostructural degeneracy predicted by the *ab initio* calculations can be found in the experimental data. The enthalpy of formation has been measured in high-temperature drop calorimetric experiments.

The bulk modulus and enthalpies of formation of $ZrMn_2$ are found to be 150 GPa and −66.6 kJ (mol of f.u.)$^{-1}$, respectively, in nice agreement with the *ab initio* calculated results. The bulk thermal expansion has been measured using a miniature capacitance dilatometer and resembles that of a typical metal. However, the temperature-dependent electrical resisitivity shows that there is a power law with $n \approx 1.1$ at low temperature quite different from simple metals which originates propably from scattering of the charge carriers on frustrated Mn moments.

The phonons have been investigated in detail by comparing results of *ab initio* calculations with neutron spectra and the experimental specific-heat data. Although experiments did not deduce any phase transition in $ZrMn_2$, from the specific heat and the phonon spectroscopy we can see that the *ab initio* data of C14 FM are in better agreement with the experimental data than those of C14 NM. This demonstrates that $ZrMn_2$ has very special spin correlations beyond FM cases, which the standard GGA spin-polarization calculations can treat. We suggest a further study including strong spin correlations (i.e., spin fluctuations or spin-geometry frustration).

ACKNOWLEDGMENTS

We acknowledge support by the Austrian Science Foundation (FWF) within projects P18054, P17226, P16250, P16778, and P16957 and by the Deutsche Forschungsgemeinschaft (DFG) within the Sonderforschungsbereich 463. One of the authors (X.-Q. C.) also gratefully acknowledges financial support from the National Natural Science Foundation of China (Grant No. 50604004).

---

*Electronic address: Martin.Rotter@univie.ac.at

[1] H. Nakamura and M. Shiga, J. Alloys Compd. **326**, 157 (2001).

[2] C. Robert, J. Bowman, and F. Brent, MRS Bull. **27**, 688 (2002).

[3] V. N. Svechnikov and V. V. Detkov, Metallofiz. Noveishie Tekhnol. **1976**, 24 (2004).

[4] T. B. Massalski, H. Okamoto, P. Subramanian, and L. Kacprzak, in *Binary Alloys Phase Diagrams*, edited by T. Massalski, H. Okamoto, P. Subramanian, and L. Kacprzak (The Materials Information Society, ASM International, Ohio, 1989), Vol. 3, p. 2629.

[5] R. M. van Essen and K. H. J. Bushow, Mater. Res. Bull. **15**, 1149 (1980).

[6] L. Y. Zhang, A. T. Pedziwatr, F. Pourarian, and W. E. Wallace, J. Magn. Magn. Mater. **68**, 309 (1987).

[7] F. Pourarian, H. Fujii, W. Wallace, V. Sinha, and H. Smith, J. Phys. Chem. **85**, 3105 (1981).

[8] V. K. Sinha and W. E. Wallace, J. Less-Common Met. **106**, 199 (1985).

[9] Ž. Blažina and R. Trojko, J. Less-Common Met. **133**, 277 (1987).

[10] H. Flandorfer, J. Gröbner, A. Stamou, A. S. N. Hassiotis, P. Rogl, R. Wouters, H. Seifert, D. Maccio, R. Ferro, G. Haidemenopoulos, L. Delaey, and G. Effenberg, Z. Metallkd. **88**, 529 (1997).

[11] S. Ishida, S. Asano, and J. Ishida, J. Phys. Soc. Jpn. **54**, 3925 (1985).

[12] S. Asano and S. Ishida, J. Magn. Magn. Mater. **70**, 39 (1987).

[13] S. Hong and C. L. Fu, Phys. Rev. B **66**, 094109 (2002).

[14] X. Q. Chen, W. Wolf, R. Podloucky, P. Rogl, and M. Marsmann, Europhys. Lett. **67**, 807 (2004).

[15] X. Q. Chen, W. Wolf, R. Podloucky, P. Rogl, and M. Marsman, Phys. Rev. B **72**, 054440 (2005).

[16] Nonius Kappa CCD Program Package COLLECT, DENZO, SCALEPACK, SORTAV, Nonius Delft, The Netherlands, 1998.

[17] G. M. Sheldrick, SHELXL-97, Program for Crystal Structure Refinement, University of Göttingen, Germany, windows version by McArdle, Natl. Univ. Ireland, Galway ed., 1997.

[18] R.-C. J. Roisnel, Mater. Sci. Forum **378-381**(1), 118 (2001).

[19] Technical Report, Oxford Instruments Analytical Ltd., UK, 2000 (unpublished).

[20] *In Desk Handbook Binary Phase Diagrams*, edited by, H. Okamoto (ASM International, Materials Park, Ohio, 2000), p. 570.

[21] F. D. Murnaghan, Am. J. Math. **49**, 235 (1937).

[22] A. P. Hammersley, ESRF Internal Report No. ESRF97HA02T, 1997 (unpublished).

[23] A. Larson and R. V. Dreele, Los Alamos National Laboratory Reports LANR86–748, 2004 (unpublished).

[24] M. Rotter, H. Müller, E. Gratz, M. Doerr, and M. Loewenhaupt, Rev. Sci. Instrum. **69**, 2742 (1998).

[25] A. Dinsdale, CALPHAD: Comput. Coupling Phase Diagrams

Thermochem. **15**, 317 (1991).

[26] M. P. Henaff, C. C. Colinet, A. Pasturel, and K. H. J. Buschow, J. Appl. Phys. **56**, 307 (1984).

[27] P. Gomozov, Y. Zasypalov, and B. Mogutnov, J. Phys. Chem. **60**, 1865 (1986).

[28] Y. Zasypalov, O. Kiselev, and B. Mogutnov, Dokl. Akad. Nauk SSSR **287**, 287 (1986).

[29] A. Turchanin, I. Tomilin, and A. Zubkov, Mater. Sci. Forum **235–238**, 367 (1997).

[30] Y. O. Esin, N. P. Bobrov, M. S. Petrushevski, and P. V. Geld, Izv. Akad. Nauk. SSSR, Met. **5**, 104 (1974).

[31] V. Witusiewicz, I. Arpshofen, H.-J. Seifert, F. Sommer, and F. Aldinger, J. Alloys Compd. **305**, 157 (2000).

[32] G. Batalin, E. Beloborodova, V. Nerubaschenko, and A. N. Shlapak, Izv. Akad. Nauk. SSSR, Met. **1**, 69 (1981).

[33] Y. O. Esin, N. P. Bobrov, M. S. Petrushevski,and P. V. Geld, J. Phys. Chem. **47**, 1959 (1973).

[34] V. Witusiewicz and F. Sommer, J. Alloys Compd. **289**, 152 (1999).

[35] X. Q. Chen, V. T. Witusiewicz, R. Podloucky, P. Rogl, and F. Sommer, Acta Mater. **51**, 1239 (2003).

[36] X. Q. Chen, W. Wolf, R. Podloucky, and P. Rogl, Phys. Rev. B **71**, 174101 (2005).

[37] K. Parlinski, Z.-Q. Li, and Y. Kawazoe, Phys. Rev. Lett. **78**, 4063 (1997); software PHONON 3.11 (2002) as implemented in MedeA, Materials Design s.a.r.l. (2003), www.materialsdesign.com